

RSC Advances



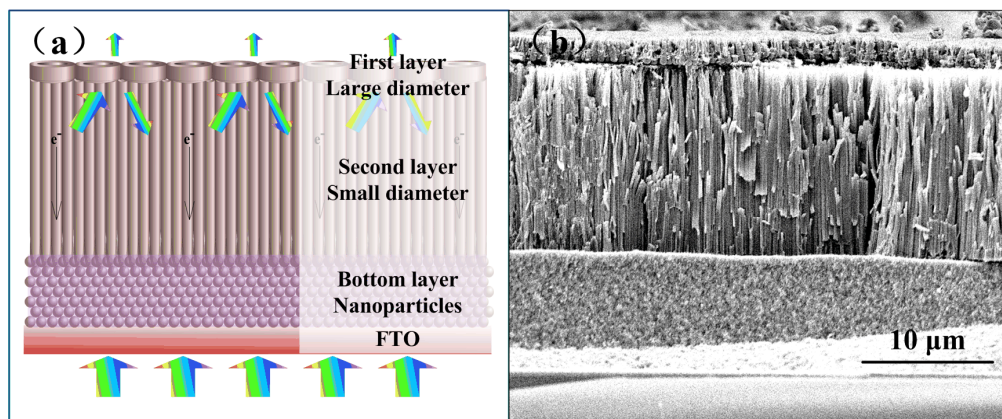
This is an *Accepted Manuscript*, which has been through the Royal Society of Chemistry peer review process and has been accepted for publication.

Accepted Manuscripts are published online shortly after acceptance, before technical editing, formatting and proof reading. Using this free service, authors can make their results available to the community, in citable form, before we publish the edited article. This *Accepted Manuscript* will be replaced by the edited, formatted and paginated article as soon as this is available.

You can find more information about *Accepted Manuscripts* in the [Information for Authors](#).

Please note that technical editing may introduce minor changes to the text and/or graphics, which may alter content. The journal's standard [Terms & Conditions](#) and the [Ethical guidelines](#) still apply. In no event shall the Royal Society of Chemistry be held responsible for any errors or omissions in this *Accepted Manuscript* or any consequences arising from the use of any information it contains.

Table of contents entry



A bi-layered TiO₂ nanotube membrane possessing fast electron transport and light scattering is used in a photoanode of DSSC.

ARTICLE

Design of multi-layered TiO₂ nanotube/nanoparticle hybrid structure for enhanced efficiency in dye-sensitized solar cells

Cite this: DOI: 10.1039/x0xx00000x

Xiaolin Liu^{a,b}, Min Guo^b, Jia Lin^a, Xianfeng Chen^{a*} and Haitao Huang^{b*}

Received 00th January 2012,

Accepted 00th January 2012

DOI: 10.1039/x0xx00000x

www.rsc.org/

A high-performance bi-layered TiO₂ nanotube membrane possessing simultaneously large surface areas for dye anchoring, excellent electron transport and strong light scattering is proposed to achieve high power conversion efficiency in dye-sensitized solar cells. The bi-layered TiO₂ nanotube arrays with different diameters are fabricated by a versatile and simple electrochemical anodization approach. The large diameter nanotube layer provides strong light-scattering while the small diameter layer provides efficient electron transport and large surface area. When the bi-layered TiO₂ nanotube membrane is attached to a conventional TiO₂ nanoparticle absorption layer to form a hybrid structured photoanode, a high power conversion efficiency of 6.52 % can be achieved.

Introduction

Nanostructured TiO₂ has been widely utilized as an efficient working electrode for dye-sensitized solar cells (DSSCs) [1-2]. Typical DSSCs are designed with TiO₂ nanoparticles (NPs) of size ~ 20 nm to attain sufficient amount of dye-loading [3, 4]. To improve the charge collection and electron transport efficiency, anisotropically one-dimensional (1D) TiO₂ nanostructures, such as nanotube arrays [5-6], nanofibers [7] and nanorods [8-9] are developed to provide direct electron transport channels. However, owing to the relatively small surface area and many electron trap states, the efficiency of DSSCs based on TiO₂ nanotubes is still lower than that of NPs. Thus numerous efforts are reported to promote these DSSC performances by improving the surface area [10-11] or crystallinity of nanotubes [12-13]. Meanwhile, implementation of scattering structure is also a versatile strategy to enhance the efficiency by promoting the light harvesting. Dispersing TiO₂ nanospheres into nanocrystallites [14-15] and the using of hierarchical TiO₂ spheres with outer diameters of 300-700 nm as the scattering layer [16-17] have been tried for increased light harvesting in DSSCs.

TiO₂ photoanode simultaneously possessing large surface area for dye-loading, superior electron transport and excellent light scattering is always sought after during the development of high performance DSSCs. Nanostructured multi-layered photoanodes have been constructed for high efficiency DSSCs, by combining nanorods or nanoparticles of various sizes with conventional NPs [18-19]. It is clear that the development of such hierarchical photoanodes which combines the advantages of the 1D nanomaterial and the conventional NPs would lead to both the efficient charge transport and the superior dye adsorption.

Herein we propose a novel multi-layered photoanode structure to enable simultaneously an efficient charge transport and a large

amount of dye-loading. In this hybrid structure, a TiO₂ NP layer is in direct contact with the FTO glass substrate to ensure a large surface area for dye anchoring. It also provides a good connection between the next bi-layered nanotube membrane and the FTO substrate. The bi-layered nanotube membrane is composed of a layer of small diameter TiO₂ nanotubes (which provide moderate surface area with efficient charge transport) and another layer of large diameter TiO₂ nanotubes (which confine unabsorbed photons close to the FTO substrate through scattering effect, facilitating electron collection). Optimization of the thickness of each layer allows us to obtain a high power conversion efficiency (PCE) of 6.52 %.

Experimental Section

The bi-layered TiO₂ nanotubes with different diameters were fabricated by anodization in a conventional two-electrode electrochemical cell. Titanium sheets were used as the working electrode while the counter electrode was Pt foil with the distance between the electrodes being 2 cm. The surface-finished Ti foil was first processed in a used (about 10 h) electrolyte (0.5 wt% NH₄F, 10 vol% H₂O and 1.5 M lactic acid in ethylene glycol, anodization electrolyte 1) to fabricate the top-layer of large diameter nanotubes. The voltage was fixed at 120 V for 10 min, and then gradually increased to 180 V for 10 min at a rate of 0.1 V/s. Then the Ti foil with the large diameter nanotubes on top was further anodized at 60 V in an ethylene glycol electrolyte containing 0.5 wt% NH₄F and 3 vol% H₂O (anodization electrolyte 2) to synthesize the second-layer of small diameter nanotubes with different lengths by changing the anodization time [20-21]. The as-grown bi-layered nanotubes were annealed at 450 °C for 2 h followed by a further anodization at 60 V to obtain free-standing bi-layered TiO₂ nanotube membranes [22]. For comparison, a single layer of small diameter TiO₂ nanotube

membrane of the same thickness as the bi-layered one was fabricated by anodizing directly at 60V in anodization electrolyte 2.

The resulting membranes were annealed at 650 °C for 2 h before they were adhered to the FTO substrate with the TiO₂ NP layer, which was synthesized via a doctor-blade method (two edges of the FTO glass were covered with 3M tape mask to control the thickness of the NP layer, followed by sliding a glass rod along the tape spacer to obtain a uniform TiO₂ NP layer). Then the prepared photoanode was further sintered at 450 °C for 2 h, followed by immersing in a dye-containing solvent (0.3 mM, N719 dye) for 3 days. A hot-melt spacer was used to separate the sensitized electrode and the counter electrode which was prepared by thermal decomposition of H₂PtCl₆ isopropanol solution on FTO glass at 380 °C for 30 min. The interspace was filled with a liquid electrolyte of DMPII/LiI₂/TBP/GuSCN in 3-methoxypropionitrile.

The microstructure and morphology of the TiO₂ nanotubes were characterized by field-emission scanning electron microscopy (FESEM, JEOL JSM-6335F). The current density-voltage (*J-V*) characteristics were analyzed using a sourcemeter (Model 2420, Keithley) under AM 1.5G illumination (100 mW cm⁻²) provided by a 300 W solar simulator (Model 91160, Newport-Oriel Instruments). Transmittance spectra were acquired using a UV-vis spectrophotometer (Model UV-2550, Shimadzu). To measure the amount of dye loading, we first immersed the sensitized electrode in 0.1 M NaOH aqueous solution for desorption. Then the concentration of desorbed dye was estimated by measuring the dye absorption at 502 nm using UV-vis spectrophotometer. The normalized IPCE values were measured with an IPCE system equipped with a Xenon lamp (Oriel 66902, 300 W), a monochromator (Newport 66902), and a dual channel power meter (Newport 2931_C) equipped with a Si detector (Oriel 76175_71580). Electrochemical impedance spectroscopy (EIS) was performed in the dark at various bias voltages with the CHI 660C electrochemical workstation (CH Instruments). The amplitude of the alternative signal was 10 mV and the frequency ranged from 10⁻¹ to 10⁵ Hz.

Result and Discussion

The FESEM images of the bi-layered TiO₂ nanotubes with different diameters are shown in Fig. 1, with large diameter nanotubes in the upper layer and small ones underneath. TiO₂ nanotubes with large diameter are normally fabricated by anodizing in an electrolyte with much water content and under a larger applied voltage [23-24]. Here, the used electrolyte added with LA was utilized to prevent too large a current density at high anodization voltages [25-26]. The diameters of the top-layer of large diameter nanotubes (LNT) are about 500 nm (viewed from the bottom) with the thickness ~2 μm. The diameter of the second-layer small diameter nanotubes (SNT) is around 120 nm, which were obtained by anodization at 60 V. As seen from the Fig.s 1c-d, the thin tube wall at the top of the top-layer LNT becomes thicker at the LNT bottom and the newly formed second-layer SNT was initiated from tube walls of the top-layer [27].

We firstly fabricated the DSSC based on SNT and NP layers according to the experimental procedure reported before [12] to examine the photovoltaic performance. The photoanodes were constructed of ~ 5 μm NP with ~ 15 μm free-standing SNT membranes which were pre-annealed at 450, 650, 750 °C,

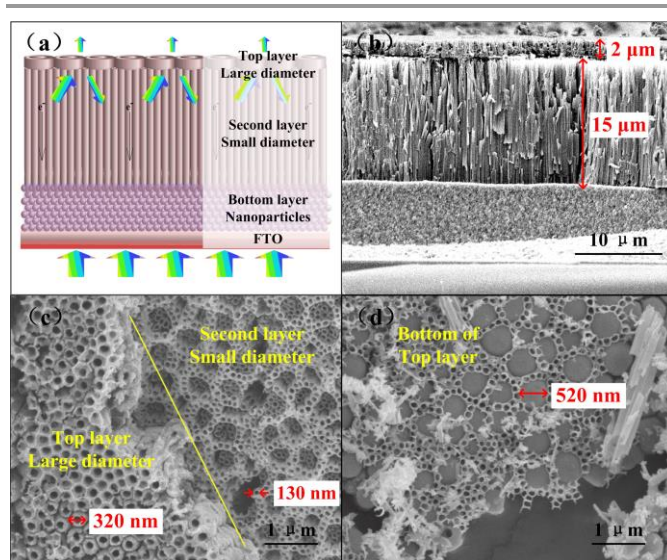


Fig. 1 (a) Schematic and (b) cross-sectional FESEM image of the multi-layered structure of the photoanode. (c) Top and (d) bottom of the top-layer of large diameter TiO₂ nanotubes.

respectively (denoted as NP5+SNT15). The XRD patterns of these photoanodes (Fig. S1a) demonstrate that no rutile phase could be found when annealed at 450 and 650 °C, while a phase transition from anatase to rutile can be observed when annealed at 750 °C. Meanwhile, the average grain size slowly increased from 33 to 41 nm and the prominent anatase peak was narrowed with increasing pre-annealing temperatures from 450 to 750 °C. The photocurrent density-voltage (*J-V*) characteristics of DSSCs based on these bi-layered photoanodes (NP5+SNT15) are shown in Fig. S1b and Table S1. The short-circuit current density (*J*_{SC}) increased with increasing pre-annealing temperature from 450 to 650 °C due to the pure anatase phase with improved crystallinity. It decreased at 750 °C due to the appearance of rutile phase. The open-circuit voltage (*V*_{OC}) attained a ~ 70 mV increment when the annealing temperature increased from 450 to 750 °C. As a result of the enhancement in both *J*_{SC} and *V*_{OC}, the efficiency of the 650 °C-annealed samples reached the maximum of 5.05%. To better illustrate the underlying mechanisms, the electrochemical properties of the DSSCs based on NP5+SNT15 photoanodes were characterized by electrochemical impedance spectroscopy (EIS) measurement in the dark at different applied bias voltages (Fig. S1c-d). The recombination times of the electrons (*τ*_n) at TiO₂/electrolyte interfaces for the 650°C- and 750°C-annealed samples are shorter than the 450°C-annealed one, owing to the enhanced crystallinity which results in decreased number of traps and faster electron transport [12]. The diameter of the medium-frequency semicircle in the Nyquist plot (Fig.S1 d) increased with increasing pre-annealing temperature, denoting larger recombination resistance (*R*_{ct}) at the TiO₂/dye/electrolyte interfaces [10, 28, 29]. Due to the decreased number of traps, lower recombination probability could be achieved. Therefore the SNT pre-annealed at 650°C with good crystallinity and pure anatase phase shows the best photovoltaic performance of DSSCs. The large diameter TiO₂ nanotubes (LNT) owns effective light scattering, and in the present work, the bi-layered TiO₂ nanotubes were successfully fabricated by growing the scattering layer (LNT) on the top of the

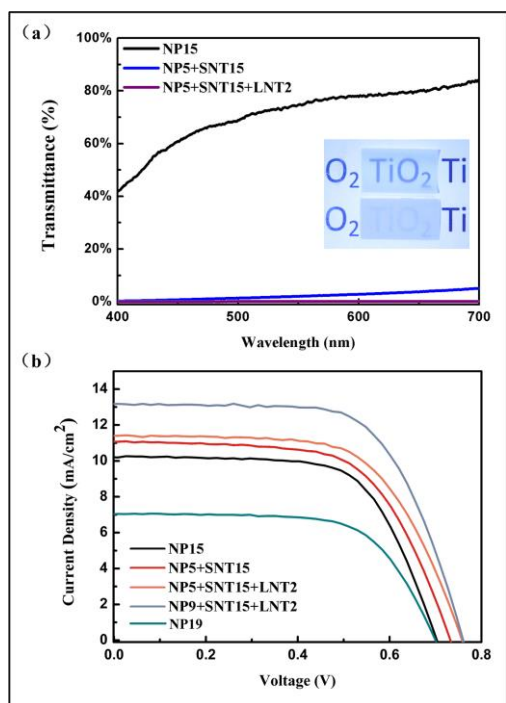


Fig. 2 (a) Transmittance of the three types of photoanodes adhered to the FTO glass substrates before the sensitization with N719. The top and bottom insets are the photos of the SNT15 and SNT15+LNT2 free-standing membranes, respectively. (b) Photocurrent-voltage curves of different photoanodes.

electron transport layer (SNT). By adhering the bi-layered TiO₂ nanotubes onto the NP layer, a three-layered photoanode was successfully fabricated, which has the following advantages: (1) the bottom NP layer provides large surface area and transparency for dye absorption; (2) the middle SNT layer guarantees superior electron transport; and (3) the upper LNT thin layer offers adequate light-scattering capability. The transmittance spectra of the three types of photoanodes on FTO glass are shown in Fig. 2a. The photoanode consisting of only the NP layer (NP15, 15 μm in thickness) shows the highest transmittance. When SNT is

Table 1. Photovoltaic properties of the DSSCs with and without the scattering layers.

Samples	Thickness in each layer (μm)	J_{sc} (mA·cm ⁻²)	V_{oc} (V)	FF	Relative Dye loading	η (%)
NP15	15	10.20	0.703	0.657	0.574	4.71
NP5+SNT15	5/15	11.07	0.732	0.623	0.419	5.05
NP5+SNT15+LNT2	5/15/2	11.39	0.758	0.627	0.474	5.42
NP9+SNT15+LNT2	9/15/2	13.17	0.760	0.651	0.582	6.52
NP19	19	7.04	0.700	0.660	0.679	3.25

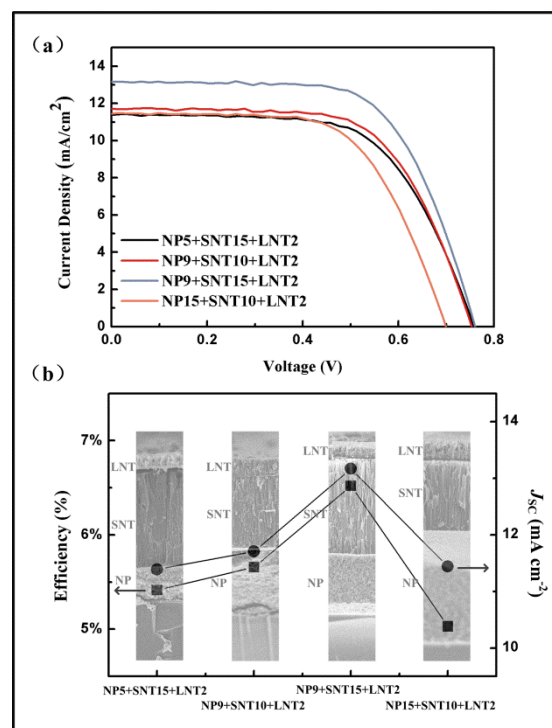


Fig. 3 (a) Photocurrent-voltage curves and (b) efficiency of power conversion of multi-layered photoanodes with different SNT and NP layer thicknesses.

attached to the NP layer, the photoanode (NP5+SNT15) shows decreased transmittance, but is still transparent. Finally, when the 2 μm LNT is used as the scattering layer, the photoanode (NP5+SNT15+LNT2) becomes translucent, showing the superior light-scattering property of LNT.

The *J-V* curves and photovoltaic properties of above samples are shown in Fig. 2b and Table 1. In our work, the optimum thickness of the TiO₂ NP reference photoanode was about 15 μm (NP15), better than a thicker NP layer of 19 μm (NP19), which is consistent with the previous results (about 12~15 μm) for high efficiency DSSCs [19, 30]. The NP15 cell shows efficiency (η) of 4.71%, with the J_{sc} of 10.20 mA·cm⁻² and V_{oc} of 0.703 mV. By applying the high temperature pre-annealed SNT to the photoanode, which has the excellent electron transport property, a noticeable improvement is achieved in V_{oc} as well as J_{sc} , resulting in an efficiency of 5.05%. The use of the light-scattering LNT layer further improves the efficiency to 5.42%. It should be noted that the use of the LNT also increases the dye loading amount. However, since the LNT is the last layer in the photoanode and the injected electrons take a longer distance (as compared to NP and SNT layers) to reach the FTO electrode, the increase in J_{sc} is not proportional to the increase in dye loading amount. The incident-photon-to-current conversion efficiency (IPCE) spectra are also depicted to further investigate the light-harvesting performance. As shown in Fig. S2, the main enhancement caused by the scattering layer occurs in the long wavelength side, which is the desired wavelength range for light harvesting enhancement in DSSCs [31-32].

The effect of thickness of each layer was further studied and several samples, namely, NP5+SNT15+LNT2, NP9+SNT10+LNT2, NP9+SNT15+LNT2, and NP15+SNT10+LNT2 (the numbers

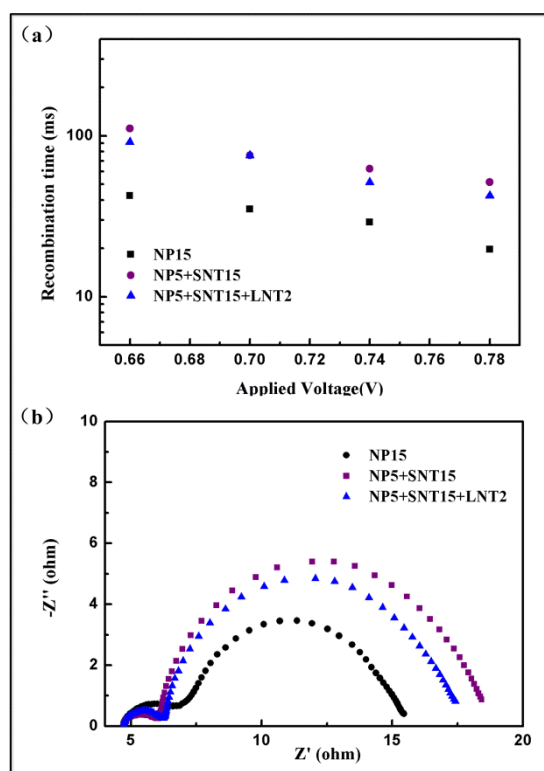


Fig. 4 (a) Electron lifetime of DSSCs as a function of bias voltage. (b) Nyquist phase plots of different types of photoanodes.

representing the thickness of each layer), are fabricated. Fig. 3 and Table S2 display the thickness dependence of the J - V curves and the photovoltaic performance of these samples. The systematically increased J_{SC} with increased NP layer thickness is resulted from the combined effect of more dye-loading due to the NP layer and the superior charge transport due to the SNT layer. The highest efficiency of 6.52% is attained in the device NP9+SNT15+LNT2 with the J_{SC} as high as $13.17 \text{ mA}\cdot\text{cm}^{-2}$. Further increasing the thickness of NP to $15 \mu\text{m}$ (NP15+SNT10+LNT2) induced decreased J_{SC} and η since the photoanode now is too thick for electron collection.

A further elucidative insight into the electrochemical behavior of the multi-layered DSSCs was also provided by the EIS measurement in the dark at different applied bias voltages. As shown in Fig. 4a, the electron recombination time (τ_n) of NP5+SNT15 is apparently longer than that of the NP based photoanode. Meanwhile, the diameter of the medium-frequency semicircle in the Nyquist plot (Fig. 4b) of NP5+SNT15 is also significantly larger than that of NP15, confirming the superior electron transport property of the high temperature annealed SNT and its contribution to the photovoltaic performance. The addition of the light-scattering layer of LNT on top of SNT slightly decreases the τ_n . Since the contribution from the strong light scattering, the efficiency of NP5+SNT15+LNT2 is higher than that of NP5+SNT15.

Conclusions

A novel multi-layered photoanode was designed to achieve simultaneously high dye-loading amount, excellent electron-

transport and strong light-scattering for DSSC applications. With a proper thickness of each layer in the photoanode, a PCE as high as 6.52% has been achieved in the NP9+SNT15+LNT2 cell, as compared with the PCE of 4.71% in a reference NP15 cell. Our work disclosed the importance of the design of multi-layered photoanode with each layer providing its different functionality in achieving high efficiency DSSCs.

Acknowledgment

The work was supported by grants received from the Research Grants Council of the Hong Kong Special Administrative Region (Project Nos. PolyU5159/13E and PolyU5163/12E) and the Hong Kong Polytechnic University (Project Nos. G-UC69 and RT5W). The work was also supported by the National Natural Science Foundation of China (Grant No. 61125503) and the Foundation for Development of Science and Technology of Shanghai (Grant No. 11XD1402600).

Notes and references

- ^a The State Key Laboratory of Advanced Optical Communication Systems and Networks, Department of Physics and Astronomy, Shanghai Jiao Tong University, 800 Dongchuan Road, Shanghai 200240, China. E-mail: xfchen@sjtu.edu.cn
^b Department of Applied Physics, The Hong Kong Polytechnic University, Hung Hom, Kowloon, Hong Kong. E-mail: aphhuang@polyu.edu.hk

† Electronic Supplementary Information (ESI) available: [details of any supplementary information available should be included here]. See DOI: 10.1039/b000000x/

- B. O'Regan and M. Grätzel, *Nature*, 1991, **353**, 737;
- A. Hagfeldt, G. Boschloo, L. Sun, L. Kloo and H. Petersson, *Chem. Rev.* 2010, **110**, 6595;
- A. Yella, H. W. Lee, H. N. Tsao, C. Yi, A. K. Chandiran, M. K. Nazeeruddin, E. W. G. Diau, C. Y. Yeh, S. M. Zakeeruddin and M. Grätzel, *Science*, 2011, **334**, 629;
- J. Ferber and J. Luther, *Sol. Energ. Mat. Sol. C.* 1998, **54**, 265;
- J. Lin, J. Chen and X. Chen, *Nanoscale Research Letters*, 2011, **6**, 475;
- C. T. Yip, H. Huang, L. Zhou, K. Xie, Y. Wang, T. Feng, J. Li and W. Y. Tam, *Adv. Mater.* 2011, **23**, 5624;
- E. Ghadiri, N. Taghavinia, S. Zakeeruddin, M. Grätzel and J. Moser, *Nano Letter*, 2010, **10**, 1632;
- J. Jiu, S. Isoda, F. Wang and M. Adachi, *J. Phys. Chem. B.* 2006, **110**, 2087;
- G. Melcarne, L. Marco, E. Carlino, F. Martina, M. Manca, R. Cingolani, G. Gigli and G. Ciccarella, *J. Mater. Chem.* 2010, **20**, 7248;
- J. Lin, X. Liu, M. Guo, W. Lu, G. Zhang, L. Zhou, X. Chen and H. Huang, *Nanoscale*, 2012, **4**, 5148;
- X. Liu, J. Lin and X. Chen, *RSC Adv.* 2013, **3**, 4885;
- J. Lin, M. Guo, G. Yip, W. Lu, G. Zhang, X. Liu, L. Zhou, X. Chen and H. Huang, *Adv. Funct. Mater.* 2013, **23**, 5952;
- Q. Ma and S. J. Liu, *Electrochim. Acta* 2011, **56**, 7596;
- J.-H. Yoon, S.-R. Jang, R. Vittal, J. Lee and K.-J. Kim, *J. Photoch. Photobio. A.* 2006, **180**, 184;
- Z. Liu, X. Su, G. Hou, S. Bi, Z. Xiao and H. Jia, *RSC Adv.* 2013, **3**, 8474;

- 16 Y.-C. Park, Y.-J. Chang, B.-G. Kum, E.-H. Kong, J. Son, Y. Kwon, T. Park and H. M. Jang, *J Mater. Chem.* 2011, **21**, 9582;
- 17 S. Dadgostar, F. Tagabadi and N. Taghavinia, *ACS Appl. Mater. Interfaces.* 2012, **4**, 2964;
- 18 H. Wu, C. Lan, J. Hu, W. Huang, J. Shiu, Z. Lan, C. Tsai, C. Su and W. Diau, *J. Phys. Chem. Lett.* 2013, **4**, 1570;
- 19 Y. Chang, E. Kong, Y. Park and H. Jang, *J. Mater. Chem. A*, 2013, **1**, 9707;
- 20 Y. Xie, L. M. Zhou and H. Huang, *Mater. Lett.* 2006, **60**, 3558;
- 21 G. Zhang, H. Huang, Y. Zhang, H. L. W. Chan, and L. Zhou, *Electrochem. Commun.* 2007, **9**, 2854;
- 22 J. Lin, J. Chen and X. Chen, *Electrochem. Commun.*, 2010, **12**, 1062;
- 23 A. Valota, D. J. LeClere, P. Skeldon, M. Curioni, T. Hashimoto, S. Berger, J. Kunze, P. Schmuki and G. E. Thompson, *Electrochim. Acta.* 2009, **54**, 4321;
- 24 L. Sun, S. Zhang, X. Sun and X. He, *Journal of Nanoscience and Nanotechnology*, 2010, **10**, 4551;
- 25 J. Ni, K. Noh, C. Frandsen, S. Kong, G. He, T. Tang and S. Jin, *Materials Science and Engineering: C*, 2013, **33**, 259;
- 26 S. So, K. Lee and P. Schmuki, *J. Am. Chem. Soc.* 2012, **134**, 11316;
- 27 B. Chen, J. Hou and K. Lu, *Langmuir*, 2013, **28**, 5911;
- 28 R. Kern, R. Sastrawan, J. Ferber, R. Stangl and J. Luther, *Electrochim. Acta*, 2002, **47**, 4213;
- 29 M. Adachi, M. Sakamoto, J. Jiu, Y. Ogata and S. Isoda, *J. Phys. Chem. B*, 2006, **110**, 13872;
- 30 S. Ito, T. Murakami, P. Comte, P. Liska, C. Grätzel, M. Nazeeruddin and M. Grätzel, *Thin Solid Films*, 2008, **516**, 4613;
- 31 F. Huang, D. Chen, X. Zhang, R. Caruso and Y.-B. Cheng, *Adv. Funct. Mater.* 2010, **20**, 1301;
- 32 Y.-J. Chang, E.-H. Kong, Y.-C. Park and H. Jang, *J. Mater. Chem. A*. 2013, **1**, 9707;